PHYSICAL REVIEW APPLIED **5,** 011001 (2016)

Rapid Driven Reset of a Qubit Readout Resonator

D. T. McClure, Hanhee Paik, L. S. Bishop, M. Steffen, Jerry M. Chow, and Jay M. Gambetta
IBM T.J. Watson Research Center, Yorktown Heights, New York 10598, USA
(Received 22 May 2015; revised manuscript received 30 October 2015; published 27 January 2016)

Using a circuit QED device, we demonstrate a simple qubit-measurement pulse shape that yields fast ring-up and ring-down of the readout resonator regardless of the qubit state. The pulse differs from a square pulse only by the inclusion of additional constant-amplitude segments designed to effect a rapid transition from one steady-state population to another. Using a Ramsey experiment performed shortly after the measurement pulse to quantify the residual population, we find that compared to a square pulse followed by a delay, this pulse shape reduces the time scale for cavity ring-down by more than twice the cavity time constant. At low drive powers, this performance is achieved using pulse parameters calculated from a linear cavity model; at higher powers, empirical optimization of the pulse parameters leads to similar performance.

DOI: 10.1103/PhysRevApplied.5.011001

Over the last decade, circuit quantum electrodynamics [1] (cQED) has become a leading architecture for constructing scalable networks of solid-state qubits, finding application in the context of not only superconducting qubits [2,3] but also spin qubits [4] and potentially other systems [5]. In this paradigm, each qubit is coupled to a resonator in which it induces a state-dependent frequency shift, allowing the qubit state to be interrogated using a pulsed tone near the resonator frequency. A great deal of research has focused on optimizing the speed and fidelity of such measurements. Most significantly, the ongoing development of quantum-limited amplifiers [6–9] has improved achievable signal-to-noise ratios enormously. The introduction of Purcell filters [10,11] has enabled the use of resonators with fast time constants, whose high bandwidth would otherwise provide a pathway for qubit relaxation via spontaneous emission (Purcell effect [12]). Some work [11,13] has also explored the use of pulse shapes with an initial overshoot in order to populate the readout resonator more quickly than the standard square pulse.

Although these improvements have made fast, high-fidelity qubit readout in cQED systems routine, relatively little attention has been devoted to the problem of returning the readout resonator to its ground state immediately after the measurement pulse. If the pulse is simply turned off, residual photons gradually exiting the resonator will continue to measure the qubit [14], preventing high-fidelity operations for a period of several time constants. Even for a resonator with a fast time constant, this delay is typically longer than the time needed for qubit control and measurement. A technique for reducing the residual population on a time scale faster than the resonator's free decay is therefore desirable in any algorithm in which qubits need to be reused shortly after measurement, e.g., error correction with surface [15,16], C4 [17], or Bacon-Shor [18] codes. A major impediment has been the fact that any such scheme needs to work in the absence of prior knowledge as to which of the two possible state-dependent resonator frequencies will be realized.

Here, we present an experimental demonstration of a driven state-independent reset of a readout resonator, using a specially designed yet simple pulse shape that we term the cavity-level excitation-and-reset (CLEAR) pulse [Fig. 1(a)]. The pulse uses short segments to "kick" the resonator rapidly from one steady-state population to another: at the beginning of the pulse, two such segments

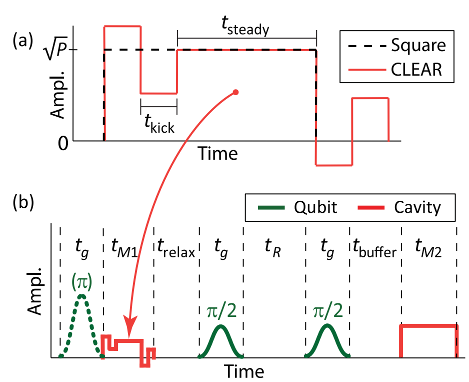

FIG. 1. (a) Schematic shape of the piecewise-constant CLEAR pulse (solid red line) with a square pulse (dashed black line) for reference. The CLEAR pulse consists of two ring-up segments of length t_{kick} followed by one segment of length t_{steady} and then two ring-down segments of length t_{kick}. (b) Pulse sequence used to extract the residual cavity population after a measurement pulse. The qubit is prepared in either the ground or excited state and then a measurement pulse (either a square pulse or a CLEAR pulse) of length t_{M1} is applied. After the measurement pulse, an adjustable delay t_{relax} precedes a pair of X_{90} pulses separated by t_R comprising a Ramsey experiment. The Ramsey experiment is followed by a delay t_{buffer} and finally a square measurement pulse of length $t_{M2} = 10\ \mu$s.

drive the population from zero to the desired steady-state value, and at the end, two more drive it back to zero. In this work, we focus on quantifying the effectiveness of the depopulating segments. Using a Ramsey experiment to extract the number of residual photons in the cavity after the pulse, we compare the performance to that of a standard square pulse. We find that for pulse powers where the cavity response remains linear, the theoretically derived CLEAR pulse shape depopulates the cavity to a negligible level in a time more than two cavity time constants faster than that needed after the square pulse. At higher powers, optimizing the pulse shape empirically using an iterative algorithm leads to equally good performance.

The experimental device is a fixed-frequency transmon qubit mounted in a 3D aluminum cavity [19] attached to the mixing chamber of a dilution refrigerator at an indicated base temperature of 10 mK. Qubit and measurement drive tones are generated using Agilent E8267D function generators and modulated using Tektronix AWG7000-series arbitrary waveform generators at a 2 GS/s sample rate. Qubit pulses are 4σ Gaussians with DRAG [20] correction. The cavity is measured in transmission, and the transmitted signal is fed to a HEMT amplifier (Low Noise Factory LNF-LNC6_20A) at 4 K using a superconducting NbTi/NbTi semirigid coaxial cable. After additional amplification at room temperature, the signal is mixed down to 16 MHz and digitally demodulated. The cavity is measured to have bare frequency $f_{\mathrm{bare}} = 10.7457$ GHz, dressed frequency $f_{\mathrm{dressed}} = 10.7594$ GHz, and linewidth $\kappa/2\pi = 1.1$ MHz (corresponding to a time constant $T_{\mathrm{cav}} = 1/\kappa = 0.14\ \mu$s). The qubit has frequency $f_{01} = 4.833\,15$ GHz, anharmonicity $\delta/2\pi = -155$ MHz, average $T_1 \approx 50\ \mu$s, and average $T_2^{\mathrm{echo}} \approx 60\ \mu$s. Preparing the qubit in the excited state shifts f_{dressed} by the cavity pull $2\chi/2\pi = -2.6$ MHz; the measurement tone is applied at the midpoint of the two frequencies, $f_{\mathrm{dressed}} + \chi/2\pi$.

The residual population after a measurement pulse can be quantified in terms of the mean cavity photon number n at some time after the end of the pulse. We use the sequence illustrated in Fig. 1(b) to extract n following an initial measurement pulse denoted $M1$. The measurement pulse is followed by a quick Ramsey experiment ($t_{\mathrm{gate}} = 8$ ns, $t_R = 0$ to 600 ns) to probe the ac Stark shift and dephasing from any residual photons [14,21]. The time t_{relax} between the end of $M1$ and the start of the Ramsey experiment can be varied to measure n as a function of time after the end of $M1$. The time t_{buffer} between the Ramsey experiment and the second measurement pulse ($M2$) is set to 400 ns to ensure that even when t_R and t_{relax} are both short, $M2$ is not corrupted by lingering photons from $M1$.

A typical Ramsey trace is shown in Fig. 2(a). The nonmonotonic modulation in both amplitude and frequency arises from the fact that the cavity population evolves during the Ramsey delay, leading to recurrences. We derive the expected form of the Ramsey trace during this transient

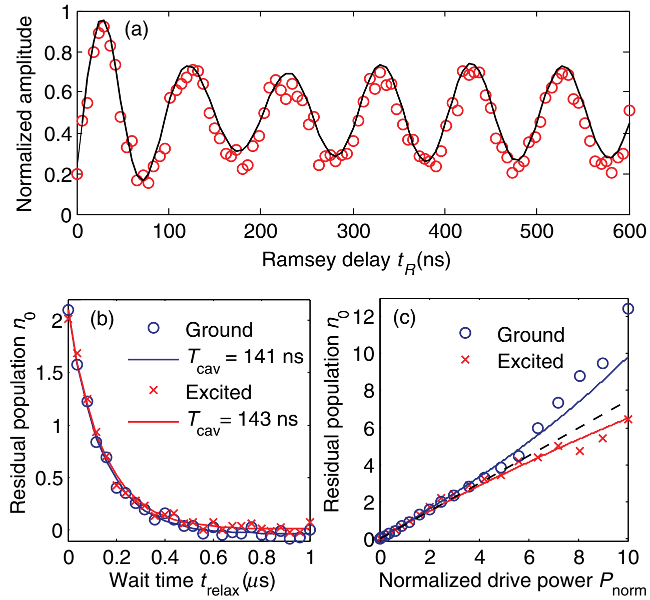

FIG. 2. (a) Sample Ramsey experiment and fit. The black curve is a fit of Eq. (1) to the data (red circles), yielding an initial cavity population of $n_0 \approx 0.9$. (b) The markers indicate n_0 versus wait time t_{relax} after a square measurement pulse with drive power $P_{\mathrm{norm}} = 2$. Here and throughout, blue and red denote experiments in which the qubit was prepared in the ground and excited states, respectively. Solid blue and red curves are exponential fits to the respective data sets. (c) n_0 versus drive power measured at $t_{\mathrm{relax}} = 40$ ns after a square measurement pulse. The dashed line indicates the prediction for a linear cavity, accounting for t_{relax}. The solid curves account for the cavity's self-Kerr nonlinearity calculated from the measured qubit and cavity parameters.

response using the positive-P-function method as in Gambetta et al. [14], where it was applied to the steady-state problem. For a Ramsey detuning Δ (here 10 MHz), decoherence rate Γ_2, and initial phase ϕ_0, the resulting functional form is

$$S(t_R) = \frac{1}{2}[1 - \mathrm{Im}\{\exp[-(\Gamma_2 + \Delta i)t_R + (\phi_0 - 2n_0\chi\tau)i]\}], \tag{1}$$

where $\tau = (1 - e^{-(\kappa+2\chi i)t_R})/(\kappa + 2\chi i)$ and n_0 is the value of n at the beginning of the Ramsey experiment. Using κ and χ obtained from frequency-domain measurements and taking $\Gamma_2 = 1/T_2^{\mathrm{echo}}$, the only free parameters are n_0 and ϕ_0. As illustrated in the figure, this function yields a good fit to the data, allowing a reliable determination of n_0. In the rest of this work, we use the extracted n_0 to quantify the residual population as a function of pulse shape, drive power, and wait time. We note that n_0 does not include the background thermal population of the cavity, which is accounted for by the Γ_2 term and is calculated from T_2^{echo} to be ~0.02 on average (assuming thermal photons are the dominant source of steady-state dephasing [22,23]).

The Ramsey fit method of obtaining n_0 is validated by using it to measure n_0 as a function of both wait time $t_{\rm relax}$ and pulse power. For simplicity, these tests are performed using square pulses for both $M1$ and $M2$, varying only the power of $M1$, denoted P as illustrated in Fig. 1(a). For convenience, we define the normalized drive power $P_{\rm norm} = P/P_{\rm 1ph}$, where $P_{\rm 1ph}$ is the steady-state drive power that yields $n = 1$, as inferred from a standard Ramsey experiment measuring the Stark shift $\Delta\omega = 2\chi n$ [14] induced by a CW tone. Figure 2(b) shows n_0 extracted from Ramsey fits as a function of $t_{\rm relax}$. Regardless of the prepared qubit state, the decay is exponential, as expected for free decay, and the time constant $T_{\rm cav}$ extracted from the best-fit curve is consistent with the value of κ obtained from frequency-domain measurements. Figure 2(c) shows n_0 as a function of $P_{\rm norm}$ at $t_{\rm relax} = 40$ ns; similar behavior is observed at all values of $t_{\rm relax}$ for which nonnegligible n_0 are measured. The dashed line indicates the expected behavior assuming a linear cavity: $n_0 = e^{-\kappa t_{\rm relax}} P_{\rm norm}$. The data exhibit a transition from a linear response at low powers to a superlinear (sublinear) response at high powers when the qubit is prepared in the ground (excited) state. This behavior is consistent with the cavity's expected self-Kerr nonlinearity [24], which shifts the cavity frequency by a negative amount K per cavity photon, pushing it closer to (farther from) the measurement frequency when the qubit is in the ground (excited) state. Approximating K in the small-δ limit as $K = 2g^4\delta(3\omega_q^4 + 2\omega_q^2\omega_r^2 + 3\omega_r^4)/(\omega_q^2 - \omega_r^2)^4$, where $\omega_q = 2\pi f_{01}$, $\omega_r = 2\pi f_{\rm dressed}$, and g is calculated as in Ref. [22], we obtain $K \approx -14$ kHz. The solid blue (red) curve indicates the expected cavity response with the qubit in the ground (excited) state, accounting for the calculated nonlinearity.

Having thus validated our method of quantifying residual photons, we then switch to a CLEAR pulse shape for $M1$. For consistency, we continue to use a square pulse for $M2$. The CLEAR pulse takes advantage of the fact that a resonator can be driven quickly from steady state S_i to steady state S_f by applying a brief kick tone between the two steady-state tones. The kick drives the resonator along a trajectory that passes through S_f, and the new steady-state drive is applied just as the resonator reaches S_f. In the presence of a qubit, the resonator can respond in one of two possible ways, necessitating the use of pairs of kicks in place of single kicks in order to achieve the desired behavior regardless of qubit state. The CLEAR pulse envelope [Fig. 1(a)] is therefore piecewise constant with five segments: two ring-up kicks, one steady-state segment (optional), and two ring-down kicks. The bandwidth of the pulse needs only to be much greater than that of the cavity, a condition readily achieved in this experiment.

There are no constraints on segment lengths in principle, but shorter segments require larger excursions in the IQ plane, so in practice the desire to stay in the linear regime sets a lower bound on the time needed. In this experiment, the lengths of the ring-up and ring-down segments are all initially fixed at $t_{\rm kick} = 150$ ns (approximately $T_{\rm cav}$). The frequency of the readout tone can also be selected arbitrarily, but using $f_{\rm dressed} + \chi/2\pi$ offers some advantages and is therefore used here. Doing so maximizes the readout signal, makes the steady-state n independent of the qubit state in the linear-response regime, and allows the CLEAR pulse segments all to be in the same quadrature. Having selected the segment lengths and drive frequency, the remaining task of determining the optimal complex amplitude for each segment is accomplished by numerically solving a driven damped harmonic oscillator model.

The cavity IQ plane trajectories produced by square and CLEAR pulses with the same steady-state amplitude ($P_{\rm norm} = 3.6$) are shown by markers in Figs. 3(a) and 3(b), respectively. For all trajectories, the time step between markers is 24 ns. Solid lines in these plots indicate

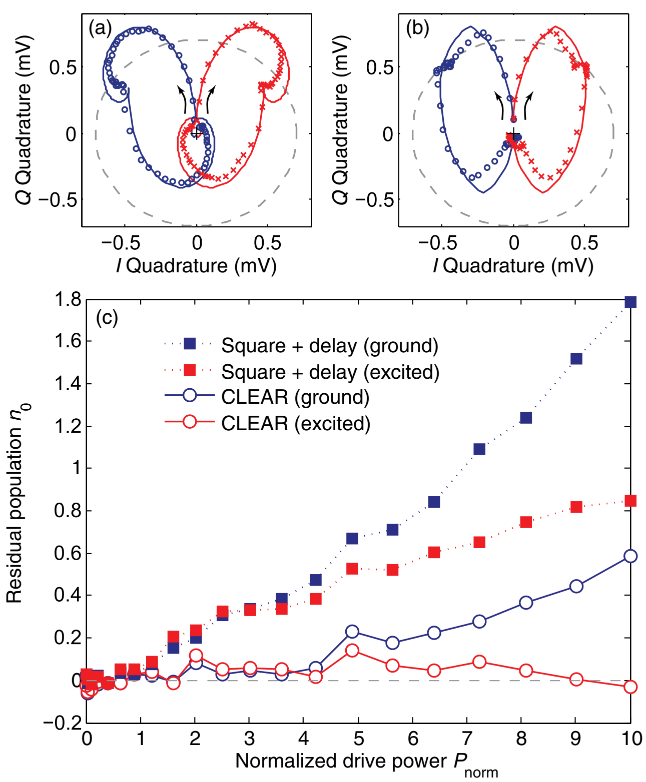

FIG. 3. (a),(b) IQ-plane cavity trajectories in response to a square pulse and CLEAR pulse, respectively. In each plot, the experimental results (markers) are superimposed on the theoretical calculations (solid curves), the dashed circle indicates the target population $n = 3.6$, the black cross indicates the origin, and the black arrows indicate the directions of the trajectories. (c) Residual cavity population versus pulse power for both square and CLEAR pulse shapes. For the CLEAR pulse, the Ramsey experiment begins immediately at the end of the pulse, while for the square pulse, a delay of approximately 300 ns is inserted to match the total length of the CLEAR pulse's two ring-down segments.

the theoretically calculated response of the cavity to each pulse, multiplied by an overall amplitude factor to match the data and adjusted to reflect the independently observed 20% thermal population of the qubit excited state (reduced by an order of magnitude on later cooldowns of this device with additional input line attenuation). We see that the experimental cavity responses track the theoretically calculated ones very well, and that compared to the square pulse, the CLEAR pulse yields more compact trajectories that reach near-steady-state populations (at both $n \approx 3.6$ and $n \approx 0$) in less time.

We quantitatively compare the performance of the CLEAR pulse to that of a square pulse using the Ramsey fit method. To provide a fair comparison, a zero-amplitude segment is appended to the square pulse to allow undriven decay during a time equivalent to the total length of the CLEAR pulse's two ring-down segments. The results are shown in Fig. 3(c). At all measurement powers, the CLEAR pulse significantly outperforms the square pulse; moreover, for drive powers that keep the cavity in the linear regime (evidenced by n_0 being independent of the prepared qubit state), the residual population immediately after the CLEAR pulse is negligible. As seen in Fig. 2(b), for drive powers in this range, negligible n_0 is not obtained until ~600 ns after a square pulse; allowing for the 300 ns taken by the ring-down segments of the CLEAR pulse, we find a net speedup of ~300 ns, or approximately $2T_{\mathrm{cav}}$. At higher powers, it appears that the cavity nonlinearity, not taken into account in calculating the optimal CLEAR pulse parameters, prevents perfect ring-down. We also find nonidealities when the lengths of the ring-down segments are reduced in an effort to shorten the ring-down time: for 120-ns ring-down segments (a 20% reduction), we find measurable n_0 even in the linear regime, as illustrated in Fig. 4(a). Further reductions in the segment lengths increase the performance degradation.

To improve the performance of the CLEAR pulse both at high powers and with shortened ringdown segments, we use an empirical technique to optimize the pulse parameters. Specifically, starting from an initial pulse shape, we randomly adjust the amplitude of one of the ring-down segments by a small amount, extract n_0 immediately after the adjusted pulse using the Ramsey technique ($t_{\mathrm{relax}} = 0$), revert the change if it did not improve n_0, and repeat until no further improvement is seen. The result of running this procedure starting from the pulse with 120-ns ring-down segments and a steady-state drive power of $P_{\mathrm{norm}} = 10$ is shown in Fig. 4(b): in fewer than 300 iterations, the pulse is optimized to yield $n_0 < 0.1$ for both possible initial qubit states. Ramsey experiments before and after running this optimization are shown in Figs. 4(c) and 4(d), revealing that coherence is preserved with the optimized pulse shape regardless of the initial qubit state. As seen in the inset of Fig. 4(b), the optimization process significantly increases the amplitudes of both ring-down segments. Extending our

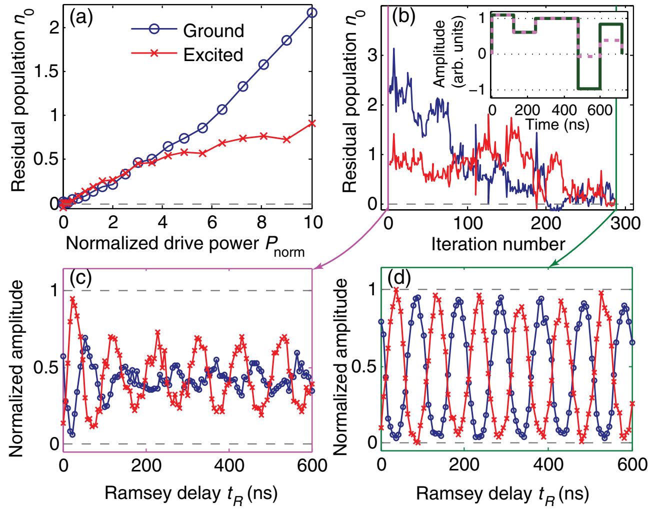

FIG. 4. (a) n_0 versus drive power for the shortened CLEAR pulse (120-ns ring-down segments), for $t_{\mathrm{relax}} = 0$. (b) Evolution of n_0 at each step of an empirical optimization algorithm for the shortened CLEAR pulse with $P_{\mathrm{norm}} = 10$. Inset: shortened CLEAR pulse shape before optimization (magenta) and after (green). (c) Ramsey traces immediately after initial shortened CLEAR pulse, yielding $n_0 \approx 2.2$ for the ground state and $n_0 \approx 0.91$ for the excited state. (d) Ramsey traces immediately after final shortened CLEAR pulse, yielding $n_0 < 0.1$ for both qubit states.

theoretical calculations to the nonlinear regime may shed light on this result and potentially eliminate the need for empirical tune-up in this regime.

In summary, using a single-qubit cQED system, a qubit-state-independent reduction in the time needed to reach a steady-state resonator population both during and after a qubit-measurement pulse is achieved by including extra constant-amplitude segments in the pulse. For low-power drives, near-perfect ring-down (quantified using Ramsey experiments) is achieved using segment amplitudes calculated from system parameters. At higher drive amplitudes, similar performance is obtained following an empirical optimization of the pulse shape. Though this demonstration used a 3D transmon, the same technique should be applicable to any cQED system; it may also be combined with machine-learning-based analysis [25] and Purcell filters to further reduce the measurement cycle time. Future areas of interest may include numerical calculation of the optimal CLEAR parameters in the nonlinear regime, the extension of this technique to resonators coupled to multiple qubits, and investigation as a possible method for implementing the resonator-induced phase gate [26] nonadiabatically.

We thank M. B. Rothwell and G. A. Keefe for device fabrication, J. R. Rozen and J. Rohrs for technical assistance, and B. Abdo for useful discussions. We acknowledge support from IARPA under Contract

No. W911NF-10-1-0324. All statements of fact, opinion, or conclusions contained herein are those of the authors and should not be construed as representing the official views or policies of the U.S. Government.

[1] A. Blais, R.-S. Huang, A. Wallraff, S. M. Girvin, and R. J. Schoelkopf, Cavity quantum electrodynamics for superconducting electrical circuits: An architecture for quantum computation, Phys. Rev. A **69**, 062320 (2004).

[2] J. Kelly, R. Barends, A. G. Fowler, A. Megrant, E. Jeffrey, T. C. White, D. Sank, J. Y. Mutus, B. Campbell, Y. Chen, Z. Chen, B. Chiaro, A. Dunsworth, I.-C. Hoi, C. Neill, P. J. J. O'Malley, C. Quintana, P. Roushan, A. Vainsencher, J. Wenner, A. N. Cleland, and J. M. Martinis, State preservation by repetitive error detection in a superconducting quantum circuit, Nature (London) **519**, 66 (2015).

[3] A. Córcoles, E. Magesan, S. J. Srinivasan, A. W. Cross, M. Steffen, J. M. Gambetta, and J. M. Chow, Demonstration of a quantum error detection code using a square lattice of four superconducting qubits, Nat. Commun. **6**, 6979 (2015).

[4] K. D. Petersson, L. W. McFaul, M. D. Schroer, M. Jung, J. M. Taylor, A. A. Houck, and J. R. Petta, Circuit quantum electrodynamics with a spin qubit, Nature (London) **490**, 380 (2012).

[5] C. Müller, J. Bourassa, and A. Blais, Detection and manipulation of Majorana fermions in circuit QED, Phys. Rev. B **88**, 235401 (2013).

[6] N. Bergeal, F. Schackert, M. Metcalfe, R. Vijay, V. E. Manucharyan, L. Frunzio, D. E. Prober, R. J. Schoelkopf, S. M. Girvin, and M. H. Devoret, Phase-preserving amplification near the quantum limit with a Josephson ring modulator, Nature (London) **465**, 64 (2010).

[7] R. Vijay, D. H. Slichter, and I. Siddiqi, Observation of Quantum Jumps in a Superconducting Artificial Atom, Phys. Rev. Lett. **106**, 110502 (2011).

[8] B. Ho Eom, P. K. Day, H. G. LeDuc, and J. Zmuidzinas, A wideband, low-noise superconducting amplifier with high dynamic range, Nat. Phys. **8**, 623 (2012).

[9] D. Hover, Y.-F. Chen, G. J. Ribeill, S. Zhu, S. Sendelbach, and R. McDermott, Superconducting low-inductance undulatory galvanometer microwave amplifier, Appl. Phys. Lett. **100**, 063503 (2012).

[10] M. D. Reed, B. R. Johnson, A. A. Houck, L. DiCarlo, J. M. Chow, D. I. Schuster, L. Frunzio, and R. J. Schoelkopf, Fast reset and suppressing spontaneous emission of a superconducting qubit, Appl. Phys. Lett. **96**, 203110 (2010).

[11] E. Jeffrey, D. Sank, J. Y. Mutus, T. C. White, J. Kelly, R. Barends, Y. Chen, Z. Chen, B. Chiaro, A. Dunsworth, A. Megrant, P. J. J. O'Malley, C. Neill, P. Roushan, A. Vainsencher, J. Wenner, A. N. Cleland, and J. M. Martinis, Fast Accurate State Measurement with Superconducting Qubits, Phys. Rev. Lett. **112**, 190504 (2014).

[12] E. M. Purcell, Spontaneous emission probabilities at radio frequencies, Phys. Rev. **69**, 674 (1946).

[13] Y. Liu, S. J. Srinivasan, D. Hover, S. Zhu, R. McDermott, and A. A. Houck, High fidelity readout of a transmon qubit using a superconducting low-inductance undulatory galvanometer microwave amplifier, New J. Phys. **16**, 113008 (2014).

[14] J. M. Gambetta, A. Blais, D. I. Schuster, A. Wallraff, L. Frunzio, J. Majer, M. H. Devoret, S. M. Girvin, and R. J. Schoelkopf, Qubit-photon interactions in a cavity: Measurement-induced dephasing and number splitting, Phys. Rev. A **74**, 042318 (2006).

[15] A. Y. Kitaev, Fault-tolerant quantum computation by anyons, Ann. Phys. (Amsterdam) **303**, 2 (2003).

[16] S. B. Bravyi and A. Y. Kitaev, Quantum codes on a lattice with boundary, arXiv:quant-ph/9811052.

[17] P. Aliferis and J. Preskill, Fibonacci scheme for fault-tolerant quantum computation, Phys. Rev. A **79**, 012332 (2009).

[18] P. Aliferis and A. W. Cross, Subsystem Fault Tolerance with the Bacon-Shor Code, Phys. Rev. Lett. **98**, 220502 (2007).

[19] H. Paik, D. I. Schuster, L. S. Bishop, G. Kirchmair, G. Catelani, A. P. Sears, B. R. Johnson, M. J. Reagor, L. Frunzio, L. I. Glazman, S. M. Girvin, M. H. Devoret, and R. J. Schoelkopf, Observation of High Coherence in Josephson Junction Qubits Measured in a Three-Dimensional Circuit QED Architecture, Phys. Rev. Lett. **107**, 240501 (2011).

[20] F. Motzoi, J. M. Gambetta, P. Rebentrost, and F. K. Wilhelm, Simple Pulses for Elimination of Leakage in Weakly Nonlinear Qubits, Phys. Rev. Lett. **103**, 110501 (2009).

[21] D. I. Schuster, A. Wallraff, A. Blais, L. Frunzio, R.-S. Huang, J. Majer, S. M. Girvin, and R. J. Schoelkopf, ac Stark Shift and Dephasing of a Superconducting Qubit Strongly Coupled to a Cavity Field, Phys. Rev. Lett. **94**, 123602 (2005).

[22] C. Rigetti, J. M. Gambetta, S. Poletto, B. L. T. Plourde, J. M. Chow, A. D. Córcoles, J. A. Smolin, S. T. Merkel, J. R. Rozen, G. A. Keefe, M. B. Rothwell, M. B. Ketchen, and M. Steffen, Superconducting qubit in a waveguide cavity with a coherence time approaching 0.1 ms, Phys. Rev. B **86**, 100506 (2012).

[23] A. P. Sears, A. Petrenko, G. Catelani, L. Sun, H. Paik, G. Kirchmair, L. Frunzio, L. I. Glazman, S. M. Girvin, and R. J. Schoelkopf, Photon shot noise dephasing in the strong-dispersive limit of circuit QED, Phys. Rev. B **86**, 180504 (2012).

[24] M. Boissonneault, J. M. Gambetta, and A. Blais, Improved Superconducting Qubit Readout by Qubit-Induced Nonlinearities, Phys. Rev. Lett. **105**, 100504 (2010).

[25] E. Magesan, J. M. Gambetta, A. D. Córcoles, and J. M. Chow, Machine Learning for Discriminating Quantum Measurement Trajectories and Improving Readout, Phys. Rev. Lett. **114**, 200501 (2015).

[26] A. W. Cross and J. M. Gambetta, Optimized pulse shapes for a resonator-induced phase gate, Phys. Rev. A **91**, 032325 (2015).